

Modeling the Nucleation and Growth Behavior of Solution Derived Thin Films

Harald Dobberstein¹ and Robert W. Schwartz²

¹ School of Materials Science & Engineering
Clemson University
Clemson, SC USA 29634-0971

² Department of Ceramic Engineering
University of Missouri-Rolla
Rolla, MO USA 65401

Keywords: modeling, sol-gel, solution deposition, transformation, nucleation, growth, substrate

ABSTRACT

A model for the prediction of microstructural evolution of solution derived thin films has been developed. The model is based on standard nucleation and growth rate expressions that have been used previously to explain transformation behavior in amorphous materials. A Basic program was written incorporating these standard analytical expressions and known material properties, such as lattice constants, moduli, and melting point, as well as calculated thermodynamic parameters, such as the volume free energy. The output of the model gives a visualization of the thin film microstructure for different boundary conditions, including substrate type, lattice matching with the film, processing temperature, and time. The utility of the model is demonstrated through comparison with experimentally obtained results for yttria-stabilized zirconia and lead zirconate titanate thin films.

INTRODUCTION

Chemical solution deposition (CSD) methods have been widely investigated for thin film formation for nearly twenty years [1] and much of this activity has been aimed at ferroelectric thin films for electronic applications [2,3]. These materials are integrated with silicon technology for ferroelectric memory applications [4], where a <111> texture is desired, as well as for pyroelectric and microelectromechanical systems applications. However, ferroelectrics are by no means the only thin film materials under development for electrical applications. Significant research has also been devoted to superconductor fabrication, especially 2nd generation coated conductors [5]. These products are based on highly oriented yttrium barium copper oxide films deposited onto buffered biaxially textured nickel substrates. Here, the fabrication of tape products with high critical current densities requires the preparation films with low angle grain boundaries [6]. Thus, there is a general need to understand how control of thin film orientation and microstructure may be exerted.

A common feature of thin film solution deposition processes is that the as-deposited film is transformed into the desired crystalline state through an amorphous intermediate [7]. It has been reported that microstructural variations that may be induced through changes in chemical precursor, processing route, or heat treatment schedule. For example, Hoffman and coworkers [8] have shown that by controlling the thickness of the deposited layer, it is possible to change the microstructure of strontium titanate films from an equiaxed configuration to a columnar structure. Another example is the work of Schwartz and colleagues [9], who have shown that surface nucleation in solution derived PZT thin films may be eliminated by adding 2,4-pentanedionate to the precursor solution. A review of the literature will reveal many such reports of processing effects on microstructure, however, few of these reports have attempted to provide a theoretical basis for the observed variations in microstructure

[10,11]. Therefore, much remains to be done in this area, and the ability to predict, or control, thin film microstructure would be of great benefit in many applications. In this paper, we report on the development of a visualization model for the prediction of microstructure in solution derived thin films. The model is based on standard thermodynamic aspects of nucleation in amorphous materials and kinetic growth rate effects that also play a role in the transformation of the film. We compare the results of the predictions with published results to demonstrate that such simulations appear feasible.

EXPERIMENTAL

Nucleation Model

The model for the nucleation and growth behavior of amorphous films was derived from the standard theory of crystallization in glasses. For the homogenous nucleation of a spherical crystallite in an amorphous film, the Gibbs free energy change is given by:

$$\Delta G_{\text{Homo}} = V \cdot (\Delta G_v + \Delta G_e) + A \cdot \gamma, \quad (1)$$

where V , A , ΔG_v , ΔG_e , and γ are, respectively, the nuclei volume, the interfacial area between the nuclei and the parent amorphous phase, the difference in volume free energy, the elastic strain energy, and the interfacial energy of the newly formed interface. From differentiation of Eqn. 1, the energy barrier for a stable homogenous nucleation event can be derived as:

$$\Delta G^*_{\text{homo}} = \frac{16\pi\gamma^3}{3(\Delta G_v + \Delta G_e)^2}. \quad (2)$$

Inhomogeneities, such as internal or external surfaces or other defects, can significantly reduce the energy barrier to nucleation. A nucleus formed in the shape of a spherical cap results in less of an increase in surface energy than homogeneous nucleation of a sphere of equivalent volume. The shape of the cap, and thus, the energy barrier to nucleation depends upon the associated surface tension forces. The relationship among these forces is given by:

$$\gamma_{sa} = \gamma_{ca} \cos(\Theta) + \gamma_{sc}, \quad (3)$$

where the subscript s stands for substrate, c indicates the crystalline nucleus, and a represents the amorphous matrix. The initial surface energy of the heterogeneous nucleation site is γ_{sa} , and γ_{ca} and γ_{sc} are the newly created surface energies between the nucleus and the matrix and the nucleus and the substrate, respectively. The contact angle between γ_{ca} and γ_{sc} is Θ . The energy barrier to nucleation is reduced in proportion to Θ , and the nucleation is said to be heterogeneous. Strain energy effects can alter interfacial energies, but because these alternations cannot be verified by experiment, they are neglected in this model. The heterogeneous nucleation barrier can be described, for $\Theta \neq 0$, by:

$$\Delta G^*_{\text{hetero}} = \Delta G^*_{\text{homo}} * f(\Theta) = \frac{16\pi\gamma^3}{3(\Delta G_v + \Delta G_e)^2} * f(\Theta), \quad (4)$$

where $f(\Theta)$ is defined as:

$$f(\Theta) = \frac{(2 + \cos\Theta)(1 - \cos\Theta)^2}{4}. \quad (5)$$

From Eqn. 5, it can be seen that the term $f(\Theta)$, and therefore, the nucleation barrier would disappear as the contact angle Θ approaches zero. However, crystallization under these conditions for standard solution processing routes is not observed due to the “kinetic barrier” to crystallization.

Rather than using a simple linear approach to describe the temperature dependence of the volume free energy on undercooling [12], this model employs an experimentally modified approach for sol-gel derived thin films, in which ΔG_v is related to the degree of undercooling (below the melting point) according to:

$$\Delta G_v = s \cdot \frac{\Delta H_f}{V_m} \cdot \left(1 - \Delta C_p (T_m - T) - \frac{T}{T_m} \left(\frac{T - T_g}{T_m - T_g} \right)^{0.66} \right), \quad (6)$$

which incorporates the glass transition temperature T_g , and an empirically derived structure factor s , which is dependent upon the precursor used. ΔH_f represents the enthalpy of fusion, V_m is the molar volume of the crystalline phase, ΔC_p is the heat capacity difference between the crystalline and amorphous phases, T_m is the melting temperature, and T is the processing temperature. For amorphous materials that do not exhibit observable glass transitions, T_g is estimated as the onset temperature of crystallization in a DSC or DTA experiment.

The difference in volume during crystallization, as well as the lattice mismatch with the substrate, creates elastic strain inside the film, and the corresponding strain energy term can be expressed as:

$$\Delta G_e = \Delta M \cdot \varepsilon^2. \quad (7)$$

ΔM is the difference in the biaxial modulus of the crystalline phase and substrate or the crystalline and amorphous phases, and ε is the lattice mismatch strain, which includes also the difference in thermal expansion. In contrast to the amorphous phase, where the modulus is assumed to be isotropic, for the crystalline phase, as well as for the substrate, the biaxial modulus also depends on crystal orientation.

The above thermodynamic expression are utilized to define a nucleation rate according to:

$$J = \rho_a \cdot f \cdot \exp\left(\frac{-\Delta G^*}{RT}\right), \quad (8)$$

where ρ_a , f , and ΔG^* are the atomic density, the transport rate between the amorphous and crystalline phase, and the critical energy barrier to nucleation.

Growth Model

Grain growth in polycrystalline films is mainly driven by the reduction of the total grain boundary area. In addition, interfacial and strain energies, or growth through intermediate phases, as seen in the transformation process of barium titanate, can significantly change the growth behavior of polycrystalline sol-gel derived thin films. These effects can alter the kinetics of grain growth in general, or selectively for certain crystal orientations. A modified expression for the growth rate can be derived as:

$$u = \frac{dr}{dt} = a \cdot f \cdot \left[\gamma_{gb} \left(\frac{1}{\bar{r}} - \frac{1}{r} \right) + \left(1 - \exp \left[\frac{-\Delta G_v + \Delta G_e - \frac{(\Delta\gamma_i + \Delta\gamma_s)}{h} + \frac{\gamma_{ca}}{r'}}{RT} \right] \right) \right], \quad (9)$$

where a , \bar{r} , r' , h , γ_i , γ_s , and γ_{gb} , are the average interatomic distance, the average grain radius, the grain radius at the interface with the substrate, the film thickness, and the interfacial, surface, and grain boundary energies, respectively.

Simulation – Microstructure Visualization

We have developed a software package based on the analytical expressions above to simulate nucleation and growth behavior in solution derived thin films. The program code is written in Basic using IBasic 1.93, a commercially available Basic program for Windows 95, 98, 2000, ME, and XP from Pyxia Development. In both simulations discussed, we started with a homogeneous amorphous phase using a cell size of 1000 x 500 atoms. For the starting conditions, we assumed random bulk nucleation, oriented interfacial nucleation (YSZ), and no surface nucleation.

RESULT AND DISCUSSION

As a first example, we have simulated the nucleation and growth of sol-gel derived yttria-stabilized zirconia (YSZ) deposited on a YSZ single crystal substrate. Fig. 1a shows our computer simulation based on the material properties summarized in Table I. For comparison, a cross-sectional TEM photomicrograph of a sol-gel derived YSZ (25% Y_2O_3) film that was deposited onto a YSZ substrate (9.5% Y_2O_3) is given in Fig. 1b [13]. The annealing conditions for both the simulation and the experiment were 60 min. at 600°C. In the simulation, we have restricted the orientation of the nuclei to one of the three principal crystallographic directions ($\langle 100 \rangle$, $\langle 110 \rangle$, and $\langle 111 \rangle$). It can be seen that the simulation predicts well the polycrystalline character within the film, with fine grains of 5-10 nm in size, as well as the formation of an epitaxially grown interface layer with a saw-tooth like morphology.

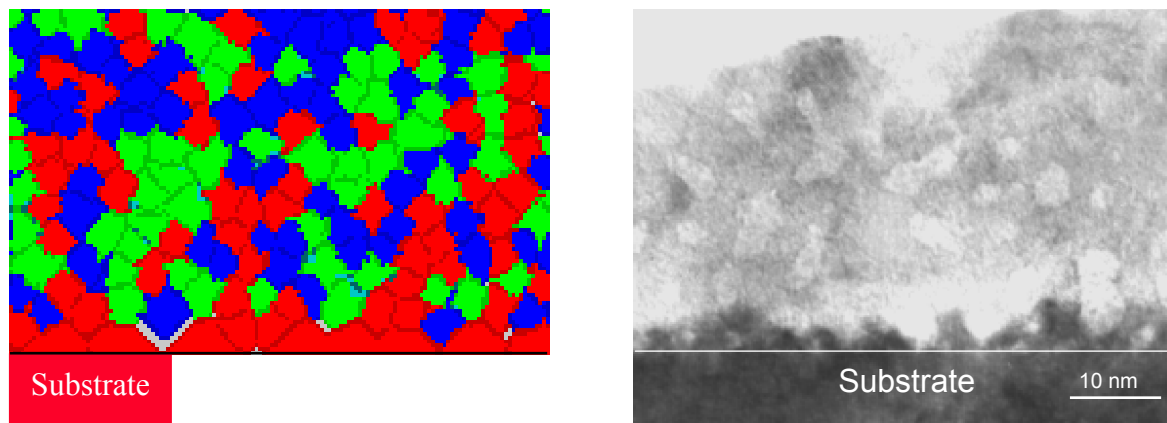


Figure 1: (a) Computer simulation of a sol-gel derived YSZ (25% Y_2O_3) film on a YSZ (9.5% Y_2O_3) single crystal substrate. Color code: $\langle 100 \rangle$ red, $\langle 110 \rangle$ green, and $\langle 111 \rangle$ blue. (b) Cross-sectional TEM micrograph of a sol-gel derived YSZ (25% Y_2O_3) film that was deposited on a YSZ single crystal substrate with a Y_2O_3 content of 9.5% [13].

Table 1. Selected material properties and calculated energies employed in the simulations for YSZ and PZT thin films.

| | Yttria Stabilized Zirconia (YSZ) | Lead Zirconate Titanate (PZT) |
|-----------------|---|---|
| s | 0.8 | 0.7 (a-f), 0.1 (f-p) ¹ |
| T _g | 420°C [14] | 370°C [15] |
| ΔH _f | 87.03 kJ/mol [16] ² | 74.63 kJ/mol [15] |
| ΔG _c | 27 MJ/m ³ [13] | 75 MJ/m ³ ³ |
| γ _{ca} | 1.01 J/m ² ⁴ | 0.87 J/m ² ⁴ |
| Θ | 90° | 90° |
| γ _{gb} | 0.9 J/m ² [19] | 0.8 J/m ² ⁵ |
| f | 8.7 x 10 ⁻³ s ⁻¹ ⁶ | 3.2 x 10 ⁻² s ⁻¹ ⁷ |
| r _c | 1.4 nm (bulk), 1.8 nm (interface) | 1.6 nm (bulk), 1.9 nm (interface) ⁸ |

¹ a: amorphous, f: fluorite, p: perovskite structure

³ Estimated using the data of [17]

⁵ Estimated using the theoretical description of [20]

⁷ Fit of data [15] using theoretical description [22]

² Value used for ZrO₂

⁴ Estimated with $\gamma_{ca} = \Psi \cdot \Delta H_f$ [18]

⁶ Fit of data [21] using theoretical description [22]

⁸ For amorphous to fluorite structure transformation

We have also simulated the nucleation and growth behavior of a sol-gel derived PZT film on a platinumized silicon wafer. In Fig. 2a-c, three snapshots are presented for different annealing times (<1, 5 and 60 min.) at 750°C. The final simulation result was compared with a real cross-sectional SEM photomicrograph of a PZT film on Pt/Ti/SiO₂/Si. The first snapshot (Fig. 2a) shows random bulk and interface nucleation of an intermediate fluorite structure, with a nucleus size of about 2 nm. In second image (Fig. 2b), perovskite phase growth begins from the substrate/film interface consuming the fine-grained intermediate fluorite phase. In Fig. 2c, the final film microstructure is shown in which the growth of the perovskite phase has progressed through the entire film. The final microstructure is a columnar in nature, in good agreement with the SEM micrograph shown in Fig. 2d.

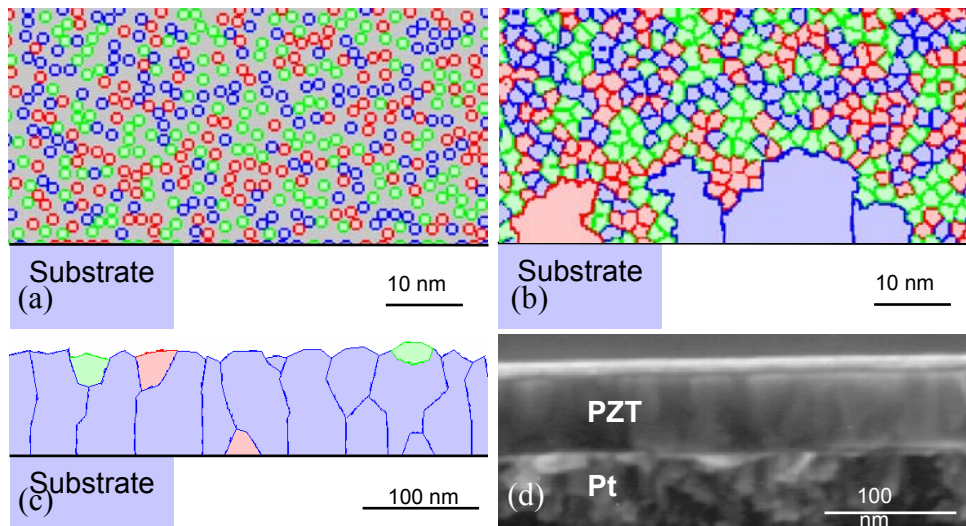


Figure 2: (a-c) Computer “snapshots” of a solution derived PZT thin film on a platinumized silicon substrate heat-treated for (a) <1 min., (b) 5 min., and (c) 60 min. at 750°C. Color code: <100> red, <110> green, and <111> blue. (d) Cross-sectional SEM photomicrograph of a sol-gel derived PZT thin film deposited onto a platinumized Si substrate [9].

CONCLUSIONS

Simulations for the microstructural evolution of solution derived YSZ and PZT thin films were presented. The model employed is based on standard expressions for nucleation and growth in amorphous materials. These expressions were incorporated into a Basic computer code that we developed to provide a visualization of microstructural evolution during heat treatment. For YSZ and PZT thin films, the simulated microstructures closely resemble those of synthesized films. These results suggest that this approach may be used effectively to predict the microstructure of solution derived films. The approach may provide a rationale for the design of processing routes to achieve particular orientations or microstructures.

ACKNOWLEDGMENTS

The authors gratefully acknowledge the technical contributions of P. G. Clem and J. A. Voigt. This research was sponsored, in part, by Sandia National Laboratories – New Mexico.

REFERENCES

1. See for example: Better Ceramics Through Chemistry I through VI, *Mater. Res. Soc. Symp. Proc.*, **32, 73, 121, 180, 271, 346** (1984 – 1994).
2. See for example: Ferroelectric Thin Films I through X, *Mater. Res. Soc. Symp. Proc.*, **200, 243, 310, 361, 433, 493, 541, 596, 655, 688** (1991 – 2001).
3. See for example: *Int. Ferro.*, Proceedings of the 1st through 12th Intl. Symp. on Integrated Ferroelectrics, **1 – 32** (1992 – 2001).
4. T. Otsuki and K. Arita, *Int. Ferro.*, **17** (1997) p. 31.
5. M. P. Paranthaman, T. G. Chirayil, F. A. List, X. Cui, A. Goyal, D. F. Lee, E. D. Specht, P. M. Martin, R. K. Williams, D. M. Kroeger, J. S. Morrell, D. B. Beach, R. Feenstra, and D. K. Christen, *J. Am. Ceram. Soc.*, **84** (2001) p. 273.
6. D. Dimos, P. Chaudhari, and J. Mannhart, *Phys. Rev. B.*, **41** (1990) p. 4038.
7. R. W. Schwartz, *Chem. Mater.*, **9** (1997) p. 2325.
8. S. Hoffmann, U. Hasenkox, R. Waser, J. L. Jia, and K. Urban, *Mat. Res. Soc. Symp. Proc.*, **474** (1997) p. 9.
9. R. W. Schwartz, R. A. Assink, D. Dimos, M. B. Sinclair, T. J. Boyle, and C. D. Buchheit, in Ferroelectric Thin Films IV, *Mat. Res. Soc. Symp. Proc.*, **361** (1995) p. 377.
10. L. Fe, G. L. Norga, D. J. Wouters, and H. E. Maes, *J. Mater. Res.*, **16** (2001) p.2499.
11. R. W. Schwartz, J. A. Voigt, B. A. Tuttle, R. S. DaSalla, R. S., and D. A. Payne, *J. Mater. Res.*, **12** (1997) p. 444.
12. D. Turnbull, *J. Appl. Phys.*, **32** (1950) p. 1022.
13. K. T. Miller, C. J. Chan, M. G. Cain, and F. F. Lange, *J. Mater. Res.*, **8** (1993) p. 169.
14. P. Duran, T. Tartaj, J. F. Fernández, M Villegas, and C. Moure, *Ceram. Int.*, **25** (1999) p. 125.
15. R. Merkle and H. Bertagnolli, *J. Mater. Chem.*, **8** (1998) p. 2433.
16. CRC Handbook of Chemistry and Physics, 66th Edition, CRC Press, Inc, Boca Raton, Florida (1985).
17. J. D. Schäfer, H. Näge, and F. Aldinger, *J. Appl. Phys.*, **85** (1999) p. 8023.
18. J. Q. Boughton and G. H. Gilmer, *J. Chem. Phys.*, **84** (1986) p. 5759.
19. A. Tsogga and P Nikolopoulos, *J. Mater. Sci.*, **31** (1996) p. 5409.
20. L. P. H. Jeurgens, W. G. Sloff, F. D. Tichelaar, and E. J. Mittermeijer, *Phys. Rev. B.*, **62** (2000) p. 4707.
21. J. S. Lee, T. Matsubara, T. Sei, and T. Tsuchiya, *J. Mater. Sci.*, **32** (1997) p. 5249.
22. H. Kumoni and F. G. Shi, *Phys. Rev. B*, **52** (1995) p. 16753.